IEEE Access
Multidisciplinary | Rapid Review | Open Access Journal

Received November 19, 2019, accepted December 24, 2019, date of publication January 3, 2020, date of current version January 14, 2020.

Digital Object Identifier 10.1109/ACCESS.2020.2963919

Complex Permittivity Measurement System for Solid Materials Using Complementary Frequency Selective Surfaces

CHIH-KUO LEE[1], SHIYU ZHANG[1], SYED SHEHERYAR BUKHARI[2], DARREN CADMAN[1], J. C. VARDAXOGLOU[1], (Fellow, IEEE), AND WILLIAM G. WHITTOW[1], (Senior Member, IEEE)

[1]Wolfson School of Mechanical, Electrical and Manufacturing Engineering, Loughborough University, Loughborough LE11 3TU, U.K.
[2]Department of Materials, University of Oxford, Oxford OX1 2JD, U.K.

Corresponding author: Chih-Kuo Lee (c.lee2@lboro.ac.uk)

This work was supported in part by the National Defense University, Taiwan, and in part by the EPRSC under Grant EP/N010493/1 through Synthesizing 3D Metamaterials for RF, Microwave and THz Applications (SYMETA) and Grant EP/S030301/1 through Anisotropic Microwave/Terahertz Metamaterials for Satellite Applications (ANISAT).

ABSTRACT This paper describes a novel method of characterizing complex permittivity using a complementary frequency selective surface (CFSS). The CFSS provides a passband behavior and the change in the passband when a material under test (MUT) is placed adjacent to the CFSS has been used for retrieving of the complex permittivity of the MUT. The complex permittivity of the MUT are determined based on the measured bandpass resonant frequency and insertion loss of the CFSS with the MUT. This is an amplitude-only method where phase measurements are not required. This technique offers a convenient, fast, low-cost and nondestructive measurement that is not restricted by the sample size or shape.

INDEX TERMS Dielectric losses, dielectric measurement, frequency selective surfaces, permittivity.

I. INTRODUCTION

A material that has the capability of storing energy when there is an external electric field applied is classified as dielectric. Dielectric materials play an important role in various engineering fields and accurate measurement of their properties is important to design the next generation of antennas and radiofrequency (RF) components. There are numerous studies on dielectric properties measurement methods. Afsar *et al.* presented a review of the dielectric property measurement methods including reflection, transmission, resonant and free space over the frequency range from 1 MHz to 1500 GHz [1]. Venkatesh and Raghavan analyzed the perturbation techniques, waveguide/coaxial transmission line methods, resonator methods, open-ended probe techniques, free space transmission techniques and microstrip transmission line methods for dielectric property characterization in [2]. Baker-Jarvis *et al.* summarized most commonly used dielectric property measurement methods according to the material category, specimen preparation, frequency band and measurement accuracy in [3]. Jilani *et al.* discussed some of the most popular dielectric property measurement methods including coaxial probe, transmission line, free space, resonant cavity and parallel plate methods [4]. They concluded that the resonant method was preferable at lower and medium frequencies while transmission line, coaxial, resonant cavity and free space methods were commonly used at higher frequencies. For high loss materials, parallel plate, coaxial probe and free space methods have shown good performance. As for low loss materials, resonant cavity methods are chosen because of their high accuracy. Generally, non-resonant methods (like transmission lines, open coax probe, and waveguides) offer wider band measurement frequency range but less accuracy compared with resonant methods (like split post resonator or dielectric resonator).

Apart from the measurement frequency range and accuracy, there are two facts which are also worth considering when choosing the appropriate measurement methods: (1) sample preparation, and (2) cost of equipment setup. Split post dielectric resonators (SPDR) [5] are a medium cost and high accuracy measurement method that suitable for dielectric substrates and thin films measurement. It can be used with or without an expensive vector network analyzer (VNA). However, there is a tradeoff in the required size of the samples. They must be square and roughly half a wavelength in size. There is also a limitation in the maximum thickness

The associate editor coordinating the review of this manuscript and approving it for publication was Boxue Du.

TABLE 1. Comparison of CFSS-waveguide and other common methods.

Method	Class	Destructive (Y/N)	Phase measurement (Y/N)	Equipment Cost	Broadband (Y/N)	Tooling error	Uncertainty (dielectric constant)	Reference
Free space	Non-resonant	N	Y	High	Y	Low	± 10 %	[7], [10]–[12].
Coaxial probe	Non-resonant	N	Y	High	Y	Low	± 3 %	[4], [7]
NRW	Non-resonant	Y	Y	High	Y	High	± 1 %	[7], [21], [22]
SPDR	Resonant	Y	N	Medium	N	Low	± 0.15 %	[5], [6]
FSS	Resonant	Y	N	Low	Y	High	± 6 %	[23]
CFSS	Resonant	N	N	Low	N	Low	± 6 %	This work

and only thin samples can be measured above 10 GHz (for instance, 0.95 mm and 0.6 mm for 10 GHz and 15 GHz measurements, respectively) [6]; the samples must have a constant thickness. The coaxial/waveguide transmission and reflection methods are easy to setup, but a VNA and phase stable cables are required for the phase measurements [7]. In addition, the MUTs have to fit exactly inside the coaxial/waveguides and the measurement accuracy is limited by the air gaps between the sample edges and coaxial/waveguide walls [8]. Open-ended coaxial probe methods are generally limited to liquids and they do not require special preparation. A large number of samples could be measured in a short time after calibration [9]. However, the air gap is problematic when measuring solid samples and the accuracy is sensitive to the phase change due to the cable movement. In addition, the cost of the equipment is substantially high due to the high precision probe and VNA. The free space method is good for high frequency, non-destructive measurements [10]–[12]. But the downside of this method is that the MUT must be large and flat. Small MUTs result in the diffraction effects at the edge of the samples, which affects the measurement accuracy. Time-gating is also required to remove reflections off nearby objects.

Recently, the microwave planar resonator structure has been used for measurement of complex permittivity due to its compact, low cost, and ease of integration with other electronic components [13]. However, the poor Q factor and low sensitivity restricted the technique from being widely used. These drawbacks of traditional planar resonator sensors were overcome by using different means like changing the materials [14], [15], and utilization of additional structures [16]–[19].

An evaluation of four different complex permittivity measurement methods including SPDR, rectangular waveguide, $TE_{01\delta}$ cavity resonator, and open resonator has been presented in [20]. It has demonstrated there were up to 10% error in measured dielectric constant values compared with the datasheet value when using these different techniques. The variation was mainly due to the change in the geometry of the MUT and the frequency range. Since the MUTs had to be cut to the measurable dimensions, the machining tolerance resulted in inaccurate geometries. Therefore, a non-destructive measurement method is highly desirable for minimizing these tooling errors.

This paper introduces a novel CFSS-waveguide technique for characterizing complex permittivity of dielectric substrates. The most significant advantage of this technique is the sample preparation is nondestructive as long as the MUT covers the CFSS area and the MUT can be in arbitrary 2D shape. Therefore, no special sample preparation is required. This CFSS technique is easier and faster than the other waveguide based methods such as Nicolson-Ross-Weir (NRW) [21], [22] and the frequency selective surface (FSS) filter method described in [23] which both require the MUTs to fit exactly inside the waveguide aperture. The ability of allowing large substrate sheet measurements makes the CFSS technique suitable for substrate quality control by assessing the complex permittivity at different locations of the same MUT without cutting or machining the MUT. Furthermore, the CFSS is fabricated by using the low-cost printed circuit board (PCB) technique with high geometry accuracy thanks to the relatively simple CFSS structure.

The CFSS design is scalable and can be adapted for conventional waveguides at different frequency ranges. Last but not the least, phase and reflection measurements are not required in the CFSS technique. It only requires transmission amplitude measurement, and therefore, it can potentially be setup without using a VNA (for instance, scalar analyzer can be used). The calibration procedure is also much simpler compared with the transmission/reflection-based methods and no special calibration kits are required. The comparison of the CFSS-waveguide method and other common methods is shown in Table 1. When compared with other common measurement methods, the advantages of the CFSS-waveguide method are that the technique is non-destructive; small or large samples of arbitrary 2D-shapes can be measured; measurements are fast; no phase is required;

and there are low equipment costs beyond standard facilities available in a microwave laboratory.

The CFSS is a miniaturized bandpass electromagnetic resonator. The dielectric constant of the MUT is determined by the bandpass resonant frequency when the MUT is placed next to the CFSS and the loss tangent is obtained from the measured insertion loss magnitude. Section II describes the overview of CFSS measurement process. Section III shows how to design the CFSS for the measurements including the investigations of the CFSS geometry effect on the bandpass resonant frequency and the Q factor optimization for a more accurate determining of the bandpass resonant frequency. Section IV explains how the MUT location when placed next to the CFSS, MUT dielectric properties, thickness and the air gap change the bandpass resonant frequency and insertion loss. The extraction procedures and recommended measurement setup are suggested due to those effects. Section V presents the design of the CFSS and discusses the measurable range of MUT size, dielectric properties and thickness. Then, the practical measurement setup and the measured results are presented in Section VI. The extracted dielectric constant and loss tangent were validated by comparing these values with the manufacturers' datasheet. Lastly, the conclusions are given in Section VII.

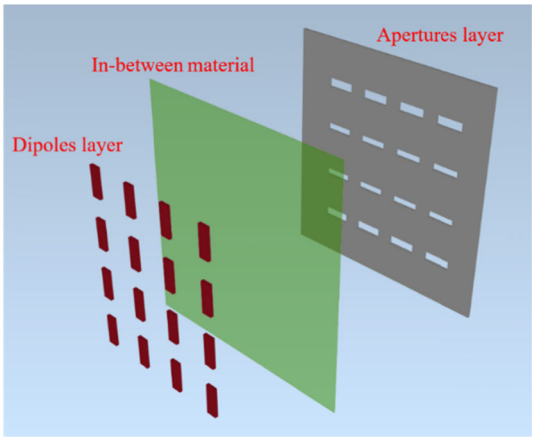

FIGURE 1. Schematic exploded view of generic CFSS.

II. OVERVIEW OF CFSS MEASUREMENT PROCESS

A. CFSS STRUCTURE

The CFSS measurement technique is a resonant method that relies on the narrow passband resonance from the CFSS structure. In an FSS, the periodic metallic elements (dipoles) on a dielectric sheet behave as band-stop filters while slots (apertures) in a metallic sheet act as band-pass filters [24]–[26]. The CFSS is a hybrid of two closely coupled FSS layers in which a layer of dipoles and a layer of apertures were etched on either side of a thin in-between dielectric material [27]. The schematic exploded view of the CFSS structure is shown in Figure 1.

The CFSS is a compact structure ($\sim\lambda/10$ depending on the geometry) and made up of two complementary FSS layers (dipoles and apertures layers) etched on either side of a thin ($\ll\lambda/100$), low-loss dielectric in-between material (IBM). The complementary structure of the CFSS can also be any shape like closed loops [28], [29] and Jerusalem crosses [30]. The CFSS is a bandpass resonator based on the Babinet's principle which states that: ''when the field behind a screen with an opening is added to the field of a complementary structure, the sum is equal to the field when there is no screen'' [31]. Although there is a thin dielectric in the CFSS case between the two FSS layers, the general underlying the Babinet concept still applies. Furthermore, the CFSS produces a lower passband resonance appearing at a frequency that is much lower than that of a single layer array (either apertures or dipoles) due to the strong fields in the IBM that is produced by the capacitively coupled layers. As a result, the CFSS realizes electrically large elements from physically small elements and creates a lower passband resonant frequency.

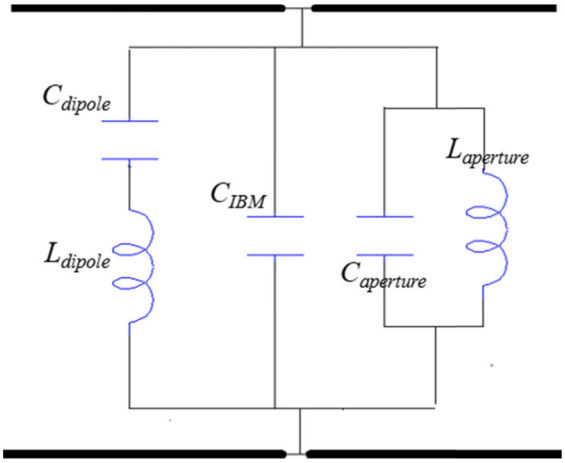

FIGURE 2. Equivalent circuit model of CFSS.

The dipoles and apertures in the CFSS are complementary (see Figure 1) and perpendicular to each other. The apertures layer is perpendicular to the electric field and acts as passband/inductive circuit, while the dipoles layer is parallel to the electric field and acts as a stopband/capacitive circuit at the same frequency if the dipoles and apertures dimensions are the same [32]. The dipole layer adds a parallel capacitance to the aperture layer, which results in the downshifting of the bandpass resonance frequency. This has been demonstrated by the equivalent circuit model presented in [33] as shown in Figure 2. The aperture layer (being a pass band structure) is represented by a parallel LC circuit, while the dipole layer (which is a stop band structure) is represented by a series LC circuit. $C_{aperture}$, $L_{aperture}$, C_{dipole} and L_{dipole} are their respective capacitance and inductance values. The coupling between the two layers is represented by a shunt capacitance C_{IBM}.

The CFSS can be presented by an equivalent parallel resonant circuit as a bandpass microwave resonator and the

resonant frequency can be calculated by (1) [34]

$$f = \frac{1}{2\pi\sqrt{LC}} \tag{1}$$

where L is the inductance and C is the capacitance.

The resonant frequency is inversely proportional to the inductance and capacitance according to (1). Therefore, the resonant frequency is expected to decrease when inductance or capacitance was added.

In the CFSS-waveguide technique, the CFSS can be excited by using conventional rectangular waveguides, and due to the compact structure and low profile, the CFSS can fit inside the waveguide to build low-cost and convenient measurement setups. A CFSS structure with 2 rows of 5 elements in both dipoles and apertures layers in the X-band (8.2 GHz to 12.4 GHz) waveguide (22.86 mm × 10.16 mm) has been simulated and compared to the individual dipoles or aperture layers. The dipoles and the aperture layer are copper and the dipoles and apertures lengths = 4 mm, widths = 1 mm and thickness = 0.02 mm. The IBM dielectric constant = 2.5, loss tangent = 0.001 and thickness = 0.1 mm. Figure 3 shows a representative transmission response of a CFSS compared to the individual layers and hence demonstrates the miniaturization achieved. The individual apertures layer or the dipoles layer have the bandpass and bandstop resonant frequency at 36.5 GHz. When they are placed either side of the IBM, the bandpass resonant frequency of the CFSS was reduced to 9.5 GHz. The CFSS bandpass resonant frequency is sensitive to adjacent dielectric materials (e.g. the MUT), and the high Q factor of the CFSS ensures a distinct resonant frequency shift. This can be used for determining the permittivity of a proximate dielectric to the CFSS.

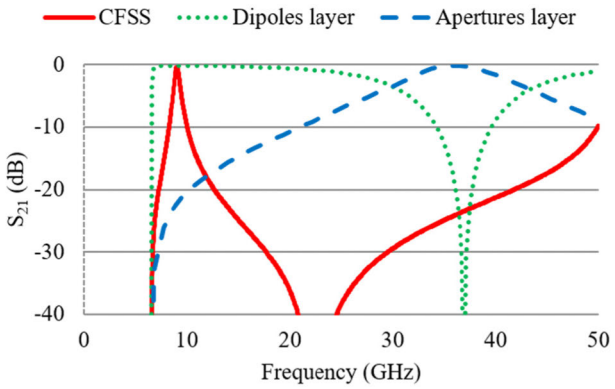

FIGURE 3. Simulated waveguide transmission responses of the CFSS, dipoles layer, and apertures layer.

B. MEASUREMENT OF MUT USING CFSS

The CFSS can be viewed as a parallel circuit as shown in Figure 2. When an MUT is placed next to a CFSS (as a bandpass resonator), it adds to the capacitance in parallel and therefore, the bandpass resonant frequency decreases. Meanwhile, the insertion loss increases due to less energy passing through.

Further, the dipole dominant component is capacitance while the aperture dominant component is inductance. Therefore, when a dielectric is close to the dipoles layer, the change in its behavior is manifested in the whole circuit capacitance. Since this capacitance adds to the capacitance of the aperture multiplied with a coupling factor, the change is more noticeable and verified using simulations in Section IV.A. However, there is a chance that the coupling might still be too small to result in an obvious frequency shift, i.e. a thin MUT with low dielectric constant despite using high dynamic range equipment and increasing the number of frequency points. One easy way to overcome this is to stack up layers of the MUT to effectively increase the MUT thickness. A thick MUT would increase the coupling and therefore results in a more significant frequency shift. The effect of the MUT thickness on the resonant frequency shift is discussed in Section IV.C

Consequently, the MUT should be placed next to the dipole layers as shown in Figure 4 to ensure the most obvious frequency shift that is beneficial for determining the dielectric properties of the MUT.

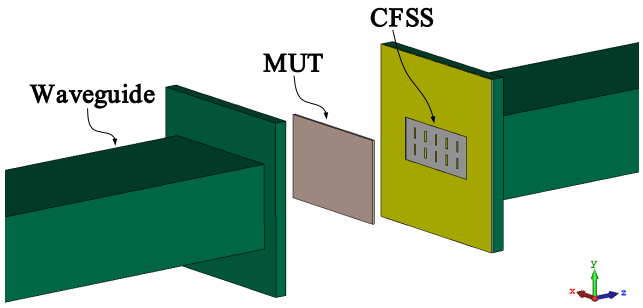

FIGURE 4. The MUT should be placed next to the CFSS dipoles layer.

Generally, the dielectric constant, ε'_r, can be found based on measurements of the resonant frequencies and the thickness of the sample:

$$\varepsilon'_r = 1 + \frac{f_o - f_s}{\mathcal{F}_1(\varepsilon'_r, t)} \tag{2}$$

where f_o is the resonance of the CFSS without the MUT, f_s is the resonance of the CFSS with the MUT, t is the thickness of the MUT. $\mathcal{F}_1$ is the function of MUT dielectric constant and thickness.

The loss tangent influences the bandpass resonant frequency and could be part of $\mathcal{F}_1$. However, the effect is very small and insignificant as will be demonstrated later in this paper. Therefore, in practical terms, $\mathcal{F}_1$ is a function of only the MUT dielectric constant and thickness.

The values of $\mathcal{F}_1$ are computed using simulations of a number of known MUT dielectric constants and thicknesses, then the $\mathcal{F}_1$ values are tabulated using (2) to form a database.

The MUT loss tangent, $\tan\delta$, can be extracted from the measured insertion losses at the bandpass resonant frequency.

The loss tangent can be found according to (3).

$$tan\delta = \frac{L_s - L_o}{\mathcal{F}_2(\varepsilon_r', t, tan\delta)} \tag{3}$$

where L_o is the insertion loss of the CFSS, L_s is the insertion loss after the MUT is placed next to the CFSS. $\mathcal{F}_2$ is the function of ε_r', t and $tan\delta$.

The CFSS technique requires three measurables: MUT thickness, bandpass resonant frequency and the insertion loss at the passband frequency. The thickness of the MUT contributes to both the frequency and the insertion loss, however, this can be easily measured and is known with a reasonable degree of accuracy. Therefore, there are two remaining measurable quantities (resonant frequency and insertion loss) and two unknowns (dielectric constant and loss tangent), which means that a two-dimensional parameter sweep of the two unknowns stored in a database will provide a unique solution.

In order to quantify those results in terms of the dielectric properties of the MUT, a database of simulated results was created using Computer Simulation Technology (CST) Microwave Studio Suite software. This database considered different MUT thicknesses, dielectric constants and loss tangents of the MUT. By matching the measured frequency and insertion loss with the simulated database of the specific MUT thickness, the dielectric properties can be extracted. This is explained in further detail in Section IV.

III. CFSS DESIGN FOR MUT MEASUREMENTS

A. CFSS GEOMETRY AND IBM

The CFSS can be fabricated by using the low-cost PCB techniques and should be designed to resonate at the upper end of the waveguide frequency band because the presence of the adjacent MUT would lower the bandpass frequency. In order to ensure the CFSS structure operated at the desired resonant frequency, simulations were carried out to investigate the effect of the CFSS parameters (including dipoles/apertures length and width, the IBM dielectric constant, loss tangent and thickness) on the bandpass resonant frequency. This section provides the design guidelines to show how the CFSS can be designed for different frequencies or if different IBMs are used.

In this paper, a CFSS that fitted in an X-band waveguide was the key requirement. The simulated frequency range was from 8 GHz to 20 GHz (Note: The range was extending beyond X-band waveguide frequency for the purpose of demonstrating the trend of the effects more clearly). In this section, there were 2 × 5 arrays of both dipoles and apertures layers as shown in Figure 4. The CFSS element dimensions were: dipole length = aperture length = 2.5 mm, dipole width = aperture width = 0.5 mm, and dipole and aperture metal thickness = 0.02 mm. IBM dielectric constant = 4, loss tangent = 0.01 and thickness = 0.05 mm. The changes in bandpass resonant frequency of the CFSS due to different IBM dielectric constants, loss tangents and thicknesses together with the dipole and aperture lengths and widths are shown in Figure 5.

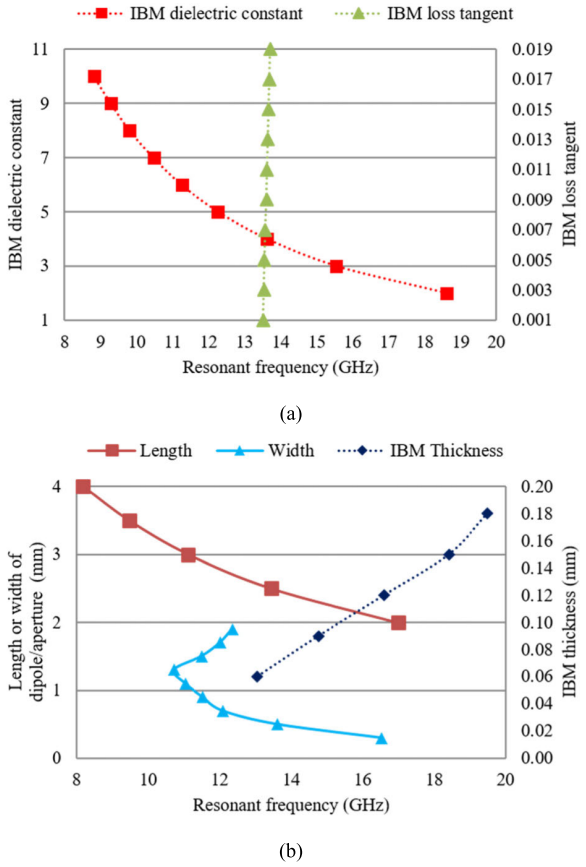

FIGURE 5. Simulated bandpass resonant frequency of the CFSS with varying: (a) IBM dielectric constant and loss tangent.; (b) length of the dipoles and apertures, width of the dipoles and apertures and the IBM thickness.

The coupling between the dipoles and apertures layers was highly affected by the IBM. The coupling became larger when the dielectric constant of the IBM was increased, and therefore the bandpass resonant frequency decreased. This is shown in red dashed line in Figure 5(a). Since the CFSS structure acted as a bandpass microwave resonator, it could be presented as an equivalent parallel resonant circuit. The relationship between the loss tangent and bandpass resonant frequency is shown in (4) [9], [34].

$$loss\ tangent = \frac{1}{Q} = \frac{\sqrt{L}}{R\sqrt{C}} = \frac{2\pi fL}{R} \tag{4}$$

where Q is the quality factor, L is the inductance, C is the capacitance, and R is the resistance. According to (4), an increased loss tangent resulted in an increased bandpass resonant frequency as shown in the green dashed line in Figure 5(a), but it is insignificant compared with the change in resonant frequency due to changes in the IBM dielectric constant.

When the IBM layer was thinner, stronger coupling existed, which should lead to a lower bandpass resonant frequency. This is shown in the dark blue dashed line in Figure 5(b).

Besides the IBM, the dipoles and apertures layers also affected the coupling. The dipoles were capacitive and hence added capacitance to the CFSS. The dipoles layer could be considered as a partial parallel conducting plate and IBM and apertures layer was the dielectric and the other conducting plate. From the parallel-plate capacitor concept, the capacitance was proportional to the surface area of the plate which was the area of the dipoles of the CFSS. Increasing the length of the dipoles expanded the surface area. Therefore, the capacitance of the CFSS was increased. According to (1), the increased capacitance resulted in decreased bandpass resonant frequency. Meanwhile, the aperture layer was inductive and added inductance to the CFSS structure. The increasing length of the apertures resulted in increased inductance and therefore decreased the bandpass resonant frequency. As a result, the bandpass resonant frequency decreased when the length of dipoles and apertures were increased as shown in the solid brown line in Figure 5(b).

The effect of bandpass resonant frequency from the width of dipoles/aperture, on the other hand, was not a linear function, see solid light blue line in Figure 5(b). The lowest bandpass resonant frequency occurred when the maximum coupling in the CFSS structure took place. The maximum coupling was found when the ratio between the width and the length of the dipoles and the apertures was 0.55 [35]. Therefore, when the length of the dipole/aperture was 2.5 mm, the lowest bandpass resonant frequency should occur when the width of the dipoles and apertures was 1.38 mm.

The simulated result of the lowest bandpass resonant frequency was found when the width of dipoles and apertures was 1.3 mm. This value verified the ratio of 0.55 between the width and length could be utilized to obtain the maximum coupling for the best miniaturization.

TABLE 2. Simulated resonant frequency effects from CFSS parameters.

Parameter	Variation	Frequency (GHz)
Length of dipoles & apertures	2.0 to 4.5 (mm)	16.9 to 6.9
Width of dipoles & apertures	0.3 to 1.3 (mm) 1.3 to 1.9 (mm)	16.5 to 10.7 10.7 to 12.4
IBM dielectric constant	2 to 10	18.6 to 8.8
IBM loss tangent	0.001 to 0.019	13.5 to 13.7
IBM thickness	0.06 to 0.18 (mm)	13.1 to 19.5

The relationship between the CFSS parameters and its bandpass resonant frequency is summarized in Table 2. It gives the guidelines for the design of the X-band CFSS structure using different PCB materials. For example, when the IBM dielectric constant increases from 2 to 10, the resonant frequency decreases from 18.6 to 8.8 GHz. As a result, when the resonant frequency is designed to be lower, the length of dipoles and apertures should be longer; the width of dipoles and apertures should be wider and approximately 0.55 times the length; and the IBM should be thinner with a higher dielectric constant to achieve the maximum level of capacitive coupling.

B. OPTIMIZATION OF THE Q FACTOR

The Q factor of the CFSS should be maximized for an accurate and precise determination of the measured resonant frequency and insertion loss since the frequency shifts are critical for the extraction of the dielectric properties in the CFSS-waveguide technique. The physical and dielectric parameters in the CFSS structure has been studied for the optimization of the Q factor in [36]. It concluded that in order to obtain the highest Q factor, the dipoles should be longer; the apertures should be shorter and narrower; the IBM should be thinner with a lower loss and a higher dielectric constant. Fewer rows of dipoles and apertures also resulted in a higher Q factor which led to one row of five dipoles and apertures in each layer in the CFSS structure was preferred for the highest Q factor [36].

A further investigation for the Q factor effect from the number of dipoles and apertures in one row has been conducted in this section. In the simulations, the CFSS structure geometry was as follows: dipoles and apertures length = 2.2 mm, dipoles and apertures width = 1.2 mm, and thickness = 0.02 mm. IBM dielectric constant = 3.54, loss tangent = 0.005 and thickness = 0.05 mm. The number of dipoles and apertures in one row was varied from 5 to 1 and this meant the Q factor increased from 56 to 101 as shown in Figure 6.

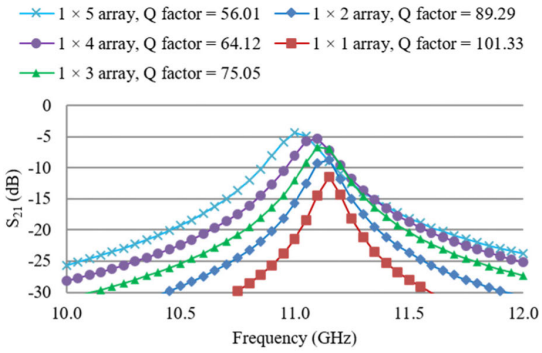

FIGURE 6. Simulated bandpass resonant frequency and Q factor from a different number of dipoles and apertures in one row.

The surface area of the dipoles and apertures both increased when the number of conductors and apertures in one row increased from 1 to 5. Hence the capacitance and inductance both increased. The Q factor is proportional to the capacitance but inversely proportional to the inductance according to (4). Since the CFSS structure is a band pass resonator, the apertures layer which acts as a band pass filter plays the dominant role. The effect from the increasing apertures' inductance was stronger than the increasing dipoles' capacitance and therefore the Q factor was expected to decrease with more elements.

Based on the above theory and results in Figure 6, the CFSS has a sharper pass band with a higher Q factor if a 1 × 1 design is used. The simulation results have demonstrated that the 1 × 1 element has the same general behavior as the 5 × 2 array. The passband was observed as indicated by Babinet's Principle, albeit the insertion loss was increased as the dimensions of the dipole and aperture are different. However, the relative change in the S_{21} behavior is the only concern in this paper and therefore the 1 × 1 element exhibited similar behavior but is advantageous in terms of having a higher Q factor. Therefore, this 1 × 1 geometry was chosen in the design and fabrication of the CFSS structure in this paper. The 1 × 1 design has the additional advantage that the distance to the edge of the waveguide is less critical which means the CFSS manufacturing and positioning errors cause less of a shift in the frequency. Furthermore, the size of the MUT can be smaller as the MUT only has to cover the area of the single dipole and slot.

IV. EFFECTS OF MUT PROPERTIES AND SIZE

In this section, the effects of the MUT dielectric properties, size and position are investigated. The CFSS with 1 × 1 dipole and aperture layers were used to investigate the effects from the MUT's dielectric properties. The dipole and the aperture layer were copper, and the dipoles and apertures lengths = 4 mm, dipoles and apertures width = 2.2 mm and thickness = 0.02 mm. The IBM dielectric constant = 3.48, loss tangent = 0.0037 and thickness = 0.48 mm. The MUT with the dimension of 24 mm × 13 mm × 0.5 mm was placed next to the CFSS structure. Electromagnetic simulations were carried out to investigate the effect of the MUT and also the air gap on the bandpass resonant frequency and insert loss.

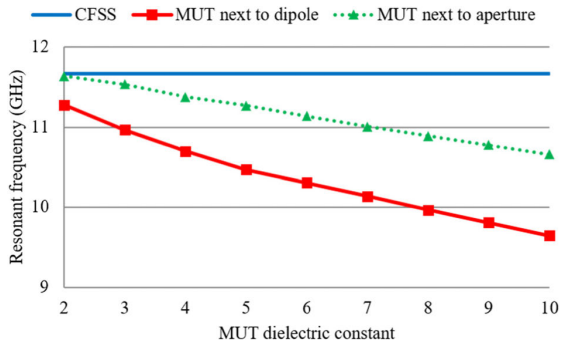

FIGURE 7. Simulated effects on bandpass resonant frequency when the 0.5 mm thick MUT was placed next to the dipole and next to the aperture layers for different dielectric constants.

A. MUT LOCATION WHEN PLACED NEXT TO THE CFSS

Capacitance is added to the CFSS when the MUT was placed next to either the dipole side or the aperture side of the CFSS structure. The bandpass resonant frequency was expected to decrease according to (1). Figure 7 shows the simulation results of the bandpass resonant frequency of the CFSS without MUT (=11.67 GHz, blue solid line), MUT placed next to the dipole side (red solid line with square markers) and next to the aperture side (green dashed line with triangle markers) when the MUT dielectric constant was varied from 2 to 10 with loss tangent 0.001. The difference between the bandpass resonant frequency of the CFSS and the MUT placed next to the dipole were larger than the difference between the CFSS resonant frequency and the MUT placed next to the aperture for all MUT dielectric constants.

For low MUT dielectric constants less than 3, if the shift of the bandpass resonant frequency peak was larger, the data collection became easier. For example, when the MUT dielectric constant was 2, the bandpass resonant frequency was 11.28 GHz and 11.64 GHz when the MUT was placed next to the dipole side and aperture side, respectively. The shift of bandpass resonant frequency was 0.39 GHz when the MUT was placed next to the dipole side and 0.03 GHz when the MUT was placed next to the aperture side.

Meanwhile, the decreasing rate of the bandpass resonant frequency was higher when the MUT was placed next to the dipole side. The decreasing rate was calculated using the shift of the bandpass resonant frequency divided by the difference of the MUT dielectric constant. For instance, with a varying MUT dielectric constant from 2 to 10, the bandpass resonant frequency decreased from 11.28 GHz to 9.65 GHz and 11.64 GHz to 10.66 GHz when the MUT was placed next to the dipole side and aperture side, respectively.

The shift of bandpass resonant frequency was 1.63 GHz for the dipole side while 0.98 GHz for the aperture side. A bigger change facilitated the extraction of the MUT dielectric constant to be more accurate when using the measured resonant frequency to match to the simulation database. Consequently, the MUT should be placed next to the dipole side to ensure the most significant frequency shift and better accuracy for determining the dielectric properties of the MUT.

B. EFFECT OF MUT DIELECTRIC PROPERTIES

The MUT dielectric constant was varied from 2 to 10 that represented the typical value of dielectric substrates. Three loss tangent values were considered when varying the MUT's dielectric constant: of 0.001, 0.01 and 0.02.

When the MUT was placed next to the dipole layer of the CFSS structure, the capacitance was increased with the increased MUT dielectric constant value, and therefore the bandpass resonant frequency was reduced. This is shown in Figure 8(a), there is a clear correlation between the dielectric constant and the bandpass resonant frequency, which allows the dielectric constant to be extracted by measuring the bandpass resonant frequency of the CFSS after placing the MUT next to the CFSS.

Figure 8(a) also shows that the curves of three different loss tangent values are almost identical. This indicated that the loss tangent has an insignificant effect on the resonant frequency, and the bandpass resonant frequency is affected primarily by the MUT dielectric constant and thickness.

The effect of varying the dielectric constant on the insertion loss from the MUT is shown in Figure 8(b). The insertion loss

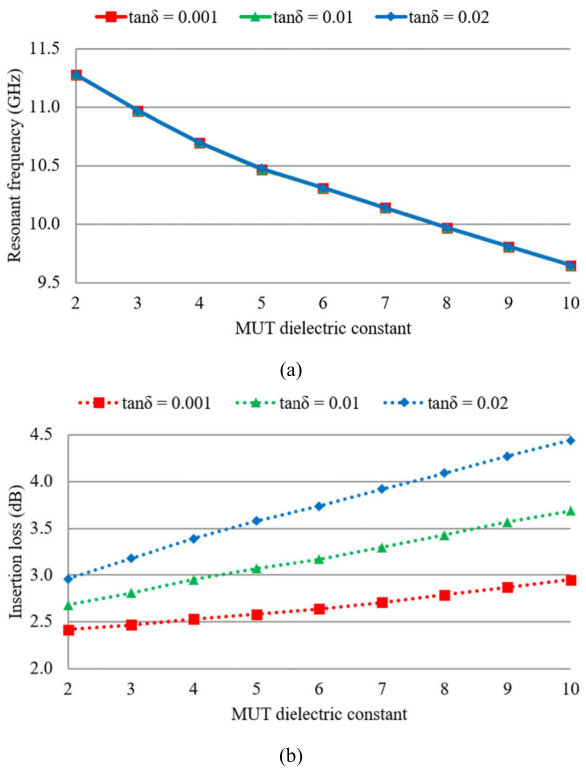

FIGURE 8. Simulated effects on bandpass (a) resonant frequency (the 3 lines overlap) and (b) insertion loss due to varying MUT dielectric constant from 2 to 10 with loss tangents (*tanδ*) of 0.001, 0.01 and 0.02.

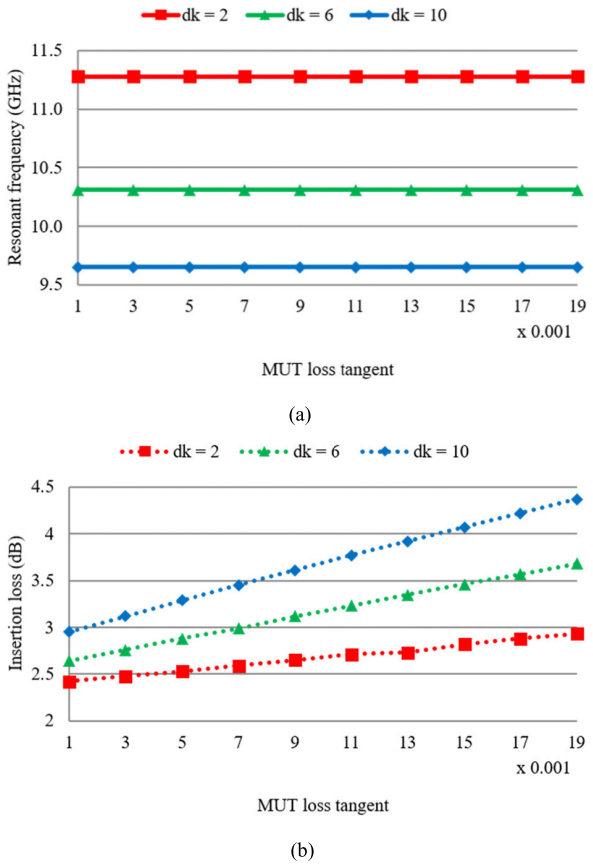

FIGURE 9. Simulated effects on bandpass (a) resonant frequency and (b) insertion loss due to varying MUT loss tangent from 0.001 to 0.019 with dielectric constants (ε_r) of 2, 6 and 10.

was increased with the increased MUT dielectric constant. This demonstrates that the insertion loss is affected by the MUT dielectric constant and the effect was larger when the MUT loss tangent was higher.

The MUT loss tangents were varied from 0.001 to 0.019. Three dielectric constants of the MUT were considered: $\varepsilon r = 2$, 6 and 10. Figure 9(a) shows that the bandpass resonant frequency was the same when the MUT loss tangent was increased from 0.001 to 0.019 in all three scenarios. The change in resonant frequency could be considered as insignificant, which confirmed the conclusion from Figure 8(a). Meanwhile, Figure 9(b) shows that the insertion loss increased by 0.51 dB, 1.04 dB and 1.42 dB for the dielectric constants of 2, 6, and 10 respectively when the MUT loss tangent increased from 0.001 to 0.019. This demonstrated the insertion loss was increased by the MUT loss tangent and the effect was larger when the MUT dielectric constant was higher.

The above studies show that the MUT's dielectric constant and loss tangent can be distinguished from the bandpass resonant frequency and insertion loss, respectively. The optimal complex permittivity measurement procedure was to first determine the MUT dielectric constant by measuring the bandpass resonant frequency because the resonant frequency was not significantly affected by the MUT loss tangent, then secondly the loss tangent can be found from the extracted dielectric constant and the measured insertion loss.

C. MUT THICKNESS LIMITATION

The MUT thickness was varied from 0.01 mm to 4.51 mm with loss tangent = 0.001. Three relative permittivities of the MUT were considered: $\varepsilon_r = 2$, 6 and 10. The capacitance was increased more when the MUT became thicker. Therefore, the bandpass resonant frequency was expected to decrease when the MUT thickness became larger. It was verified by simulations as shown in the solid lines in Figure 10(a) and the patterns from three different MUT dielectric constants also showed the bandpass resonant frequency converges when the MUT thickness increased. The convergence was clearer when the MUT dielectric constant was lower. However, the peak of the bandpass resonant frequency became hard to determine when MUT thickness was thicker than 3.51 mm and 2.51 mm for MUT dielectric constant = 6 and 10, respectively.

Additional simulations using MUT loss tangent = 0.02 with dielectric constants of 2, 6 and 10 when varying the thickness from 0.01 mm to 4.51 mm were conducted, and the bandpass resonant frequency results were the same as the MUT loss tangent was 0.001, see dashed lines in Figure 10(a). It indicated the bandpass resonant frequency was not affected by MUT loss tangent no matter what the MUT thickness was which also confirmed the conclusion from Figure 8(a).

The insertion loss was expected to increase when the MUT thickness increased since less energy passed through.

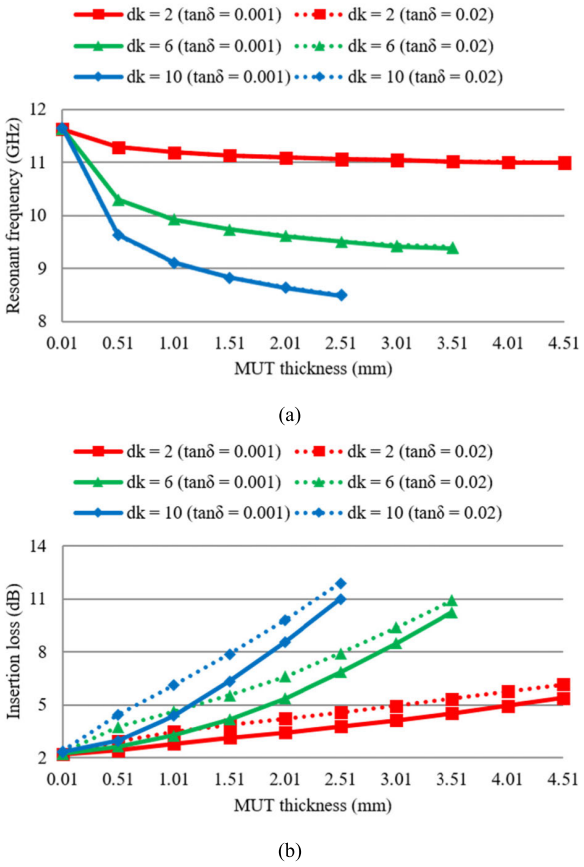

FIGURE 10. Simulated effects on bandpass (a) resonant frequency and (b) insertion loss due to varying MUT thickness from 0.01 mm to 4.51 mm with dielectric constants (dk) of 2, 6 and 10.

The simulated results as shown in the solid lines in Figure 10(b) demonstrated the insertion loss increased when the MUT thickness increased. The change in the insertion loss became larger when the MUT dielectric constant was higher. As the MUT became lossier (loss tangent = 0.02 instead of 0.001), the insertion loss became larger as shown in the dashed lines in Figure 10(b).

D. EFFECT OF AIR GAP

The air gap between the CFSS structure and the MUT is a source of measurement uncertainty. The presence of the air gap increases the bandpass resonant frequency, which leads to a lower measured dielectric constant. To quantify this effect, different air gaps including 0, 0.1, 0.2 and 0.3 mm between the CFSS structure and MUT were simulated. The same CFSS in the previous section and a MUT CER-10 (dielectric constant = 10; loss tangent = 0.0035) with the dimension of 24 mm × 13 mm × 0.59 mm were used to investigate the effects of air gap. The bandpass resonant frequencies of different air gaps are shown in Figure 11. The bandpass resonant frequency became higher when the air gap increased.

A 0.1 mm air gap between the CFSS dipole and MUT resulted in a bandpass resonant frequency of 10.65 GHz while no air gap resulted in 9.51 GHz. Hence, the extracted

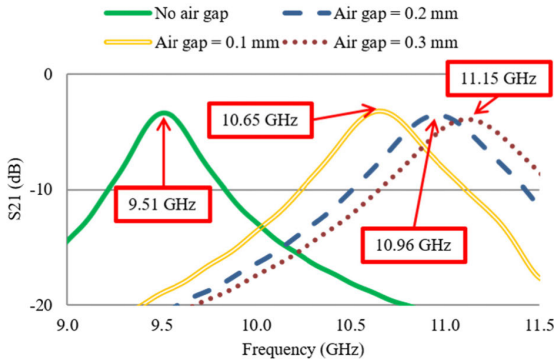

FIGURE 11. Simulated bandpass resonant frequencies due to different air gaps including 0, 0.1, 0.2 and 0.3 mm between the CFSS and MUT.

relative permittivity of the MUT was lower than the datasheet value due to the air gap effect. For example, the extracted relative permittivity of MUT CER-10 was 9.16 instead of 9.51 (extracted value with no air gap) if there was a 0.1 mm air gap between the CFSS structure and the MUT. Therefore, the minimization of the effects of the air gap is required for an accurate measurement result. Two possible solutions were considered to achieve this objective: 1) The area of the CFSS dipole that the MUT touched needs to be flat and solid to avoid any air gap when the MUT was pressed onto the CFSS. 2) The waveguide sections could be positioned vertically to allow the MUT to be pressed onto the CFSS tightly. Both solutions were considered for the measurement setup in next section.

V. CFSS DESIGN AND MEASURABLE MUT RANGE

A. DESIGN OF THE CFSS

A single dipole and single aperture CFSS were used for maximizing the Q factor and the dimensions were optimized to have the resonant frequency at the upper end of the X-band frequency range. The CFSS structure was designed using Rogers RO4350B [37] (dielectric constant = 3.48; loss tangent = 0.0037 and thickness = 0.48 mm) as the IBM. The CFSS geometry were dipole length = aperture length = 4 mm, dipole width = aperture width = 2.2 mm and metal thickness = 0.02 mm.

B. MEASURABLE MUT SIZE, DIELECTRIC PROPERTIES AND THICKNESS

Simulations for the designed CFSS were conducted to verify the minimum MUT size where accurate dielectric properties can be extracted. The minimum size of the MUT for practical measurements needed to be larger than the smallest dimension of the X-band waveguide aperture (10.16 mm) to allow the waveguide to press onto the CFSS to minimize the air gap effects. To investigate the minimum measurable sample size, the MUT (11 mm in Z axis and thickness 0.5 mm) was simulated while the width (Y axis) was varied from 1 mm to 11 mm with four different dielectric constants: 2, 6, 10 and 20. The bandpass resonant frequency maintained the

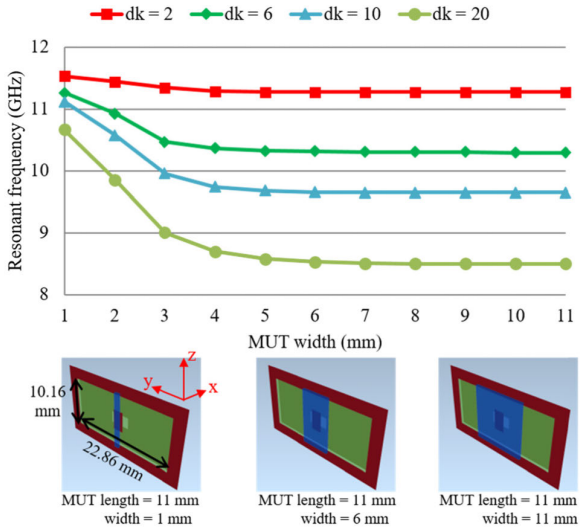

FIGURE 12. Simulated effects on bandpass resonant frequency due to varying MUT width (in blue) from 1 mm to 11 mm with length 11 mm, thickness 0.5 mm and dielectric constants (dk) 2, 6, 10 and 20.

same value when the MUT width was greater than 6 mm as shown in Figure 12.

Therefore, the MUT can be any size and shape as long as the area approximates the required size of 11 mm × 6 mm for this specific design of CFSS. The reduced minimum measurable sample size is an advantage compared to a multi-element CFSS. It is worth noting that the technique is not limited to rectangular shapes and the MUT can have any shape. However, the MUT should have the same thickness and be flat surfaces on both sides. This freedom to measure different shapes as well as small and large samples is a key advantage of this technique.

The range of the measurable MUT dielectric constants is affected by the MUT thickness. The bandpass resonant frequency decreases when the MUT thickness or dielectric constant increases, and the minimum bandpass resonant frequency is restricted to the lowest X-band frequency 8.2 GHz. As a result, the maximum measurable MUT dielectric constant is expected to decrease when the MUT thickness increases. This has been verified using simulations as shown in red line in Figure 13. The minimum detectable MUT dielectric constant for different thickness is determined when the bandpass resonant frequency shift is more than 0.01 GHz which can be used to compare with the database. Note, the simulated results show frequency shifts of less than 0.01 GHz when the MUT thickness was less than 0.25 mm, 0.1 mm and 0.04 mm with the MUT dielectric constant less than 1.1, 1.2 and 1.3, respectively. For this specific design of CFSS, the limit of the measurable MUT dielectric constant is 1.2 to 88, 1.1 to 15 and 1.1 to 12 when the MUT thickness is 0.1 mm, 1 mm and 2 mm, respectively.

The maximum measurable MUT thickness for this designed CFSS can also be found using Figure 13 if the expected MUT dielectric constant is known. For example,

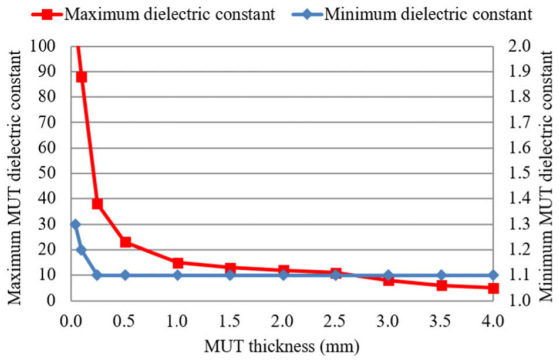

FIGURE 13. Simulated measurable maximum and minimum MUT dielectric constant of the designed CFSS when MUT thickness varied from 0.04 mm to 4 mm.

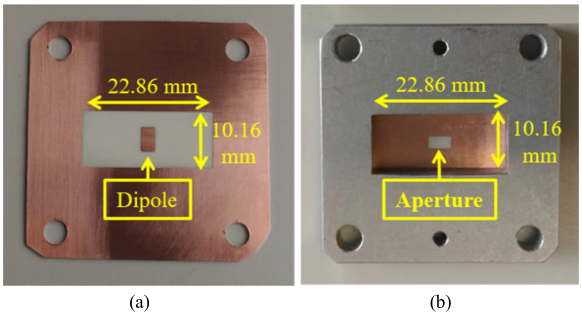

FIGURE 14. Fabricated CFSS structure in (a) dipole side view and (b) aperture side view (Note: the flange represents the waveguide section).

when the MUT dielectric constant is less than 11, the maximum measurable MUT thickness is 2.5 mm. The minimum detectable MUT thickness is determined when the bandpass resonant frequency shift is more than 0.01 GHz for the comparison with the database. This lower limit was found to be 0.04 mm when the MUT dielectric constant was greater than 1.3.

The range of measurable MUT loss tangents is dependent on both the MUT dielectric constant and thickness. The maximum measurable MUT loss tangent is determined when the CFSS no longer had a clear passband. The minimum detectable MUT loss tangent is defined when there is an insertion loss change greater than 0.01 dB when compared with the insertion loss of the CFSS only. If an MUT thickness of 1 mm is used as an example, the limit of the minimum detectable MUT loss tangent is between 0.001 to 1 and 0.001 to 0.32 when the MUT dielectric constant is 3 and 15, respectively.

VI. MEASUREMENT SETUP AND RESULTS

A. SETUP

The designed CFSS structure was fabricated as shown in Figure 14. Three different MUTs were used for the validation: TLX-0 [38], RO4360G2 [39] and CER-10 [40] with approximate dimensions of 40 mm × 40 mm. In order to minimize the effects of the air gap, a 0.48 mm thickness

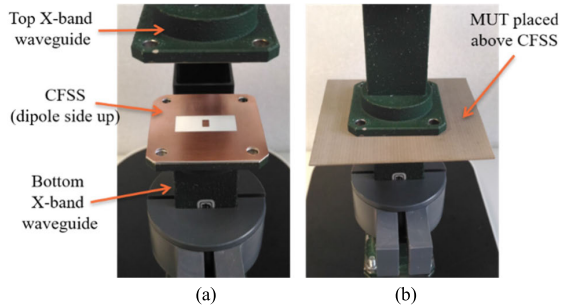

FIGURE 15. CFSS measurement: (a) the CFSS is placed on top of the bottom X-band waveguide; (b) top X-band waveguide section moved down and pressed the MUT onto CFSS tightly.

IBM was used for physically supporting the dipole against the MUT when the waveguides were pressed together during the measurements.

Meanwhile, the waveguide sections were orientated vertically, and care was taken during the measurements to minimize the air gaps. The CFSS was fitted tightly in the waveguide as shown in Figure 15(a).

The MUT was placed on top of the CFSS dipole layer and pressed onto the CFSS tightly by the top X-band waveguide section to eliminate the air gap effect, shown in Figure 15(b). The bandpass resonant frequency and insertion loss were measured after the top waveguide section was moved down. Figure 15(b) also shows the nondestructive advantage of this technique as the maximum MUT size is not limited.

TABLE 3. Datasheet and measured dielectric properties of TLX-0, RO4360G2 and CER-10 using CFSS-waveguide method.

		MUT		
		TLX-0	**RO4360G2**	**CER-10**
Measured S_{21} results	Thickness (mm)	0.57	0.51	0.59
	Bandpass resonant frequency (GHz)	11.04	10.31	9.57
	Insertion loss (dB)	4.83	4.95	7.32
Datasheet properties	Dielectric constant	2.45 ± 0.04	6.15 ± 0.15	10.00 ± 0.50
	Loss tangent	0.0019	0.0038	0.0035
CFSS extracted properties	Dielectric constant	2.53	5.76	9.51
	Loss tangent	0.0045	0.0055	0.0076

B. MEASURED RESULTS

The proposed technique was validated by comparing the measured complex permittivity of the MUTs with manufacturers' datasheet values. As described in Section II. B, by matching the measured frequency and insertion loss with the simulated database, the dielectric properties can be extracted. The manufacturers' datasheet values of dielectric constant and the loss tangent of the MUT together with the measured results from CFSS-waveguide method are shown in Table 3.

Comparing the extracted dielectric constant to the manufacturer's datasheet values of MUTs, accuracies of within 6 % were obtained for all three MUTs. The extracted loss tangents of these low-loss MUTs by using this technique were slightly higher (by up to 0.004) than the datasheet values.

To check the repeatability of the measurement process, the measured bandpass resonant frequency and insertion loss of the CFSS structure without the MUT were recorded once a day over five different days. The results were found to be very repeatable which demonstrates that the measurement setup was reliable. The measured bandpass resonant frequency was 11.67 GHz within ± 0.01 GHz, and the insertion loss was 2.31 dB with ± 0.01 dB. Each MUT was also measured by randomly placing the MUT on the CFSS once a day over five different days. The variation of the bandpass resonant frequency and insertion loss with the same MUT were within ± 0.01 GHz and ± 0.15 dB, respectively. This demonstrated that the air gap, waveguide section discontinuity and position of the sample did not create significant problems. For the CFSS in this paper, a shift of 0.01 GHz would lead to an uncertainty in the dielectric constant of 0.03 and a change in the insertion loss of 0.15 dB would lead to an uncertainty of the loss tangent of 0.005. This quantifies the level of repeatability of the measurement system.

When the MUT was placed next to the CFSS, errors from the discrepancy between CST and the actual measurement were expected since the environment in practice was not always perfect like in the simulations. A practical way to reduce the uncertainty due to the environment was to test and develop the system using reference MUTs with known dielectric properties. The extracted dielectric properties of the reference MUT were compared with the database and the discrepancy was used for the consideration of measurement for unknown MUTs. These three MUTs used in this section are capable of being the control MUTs for future measurements.

VII. CONCLUSION

A novel complex permittivity measurement system of using a CFSS structure has been demonstrated. The CFSS design concept; elements optimization for improving the measurement accuracy; and the measurement procedure have been described in detail and validated through the experimental measurements. The results have shown a good agreement between the measured complex permittivity and the manufacturer data.

The CFSS-waveguide method is useful for the determination of dielectric constants from the bandpass resonant frequency as a resonant method. The difference of the Q factor was small when the loss tangent varied in the simulation which made the extraction of loss tangent from the measured Q factor difficult. Therefore, the loss tangent was extracted from the insertion loss instead of the Q factor like most resonant methods. The MUTs measured in this paper are very low loss samples. The CFSS technique demonstrates that the losses are very small. Trying to measure such small values of loss tangent is challenging for any technique to

do reliably. Low loss materials were measured in this paper and the uncertainties of the extracted dielectric constant and loss tangent were within 6 % and 0.004, respectively. The system can potentially measure reasonably lossy MUTs with loss tangents of the order 0.3 to 1 depending on the thickness and relative permittivity.

It worth noting that the sample size can be any shape or size as long as it is larger than the CFSS element. Extending the MUT to beyond the edges of the waveguide in one dimension allows better control of the air gap effects. The MUT should have a uniform thickness, although in principle MUTs that are not exactly flat could also be measured.

The CFSS-waveguide measurement method is nondestructive, convenient and low-cost to set up. The air gap effect has been minimized by taking the advantages of the waveguide flange, which ensure the MUT is tightly pressed to the CFSS surface. This technique is capable of measuring flat dielectric substrate sheets with arbitrary dimensions, which makes this technique a good candidate for quality control at different locations of the same dielectric substrate.

ACKNOWLEDGMENT

The authors would like to thank Taconic Advanced Dielectric Division and Rogers Corporation for providing the test materials.

REFERENCES

[1] M. N. Afsar, J. R. Birch, R. N. Clarke, and G. W. Chantry, "The measurement of the properties of materials," *Proc. IEEE*, vol. 74, no. 1, pp. 183–199, Jan. 1986.

[2] M. S. Venkatesh and G. S. V. Raghavan, "An overview of dielectric properties measuring techniques," *Can. Biosyst. Eng.*, vol. 47, no. 4, pp. 15–30, 2005.

[3] J. Baker-Jarvis, M. Janezic, and D. Degroot, "High-frequency dielectric measurements," *IEEE Instrum. Meas. Mag.*, vol. 13, no. 2, pp. 24–31, Apr. 2010.

[4] M. T. Jilani, M. Z. Rehman, A. M. Khan, M. T. Khan, and S. M. Ali, "A brief review of measuring techniques for characterization of dielectric materials," *Int. J. Inf. Elect. Eng.*, vol. 1, no. 1, pp. 1–5, Dec. 2012.

[5] T. Nishikawa, K. Wakino, H. Tanaka, and Y. Ishikawa, "Precise measurement method for complex permittivity of microwave dielectric substrate," in *Proc. Conf. Precise Electromagn. Meas.*, vol. 9, 1988, pp. 155–156.

[6] QWED Company. *Split Post Dielectric Resonators (SPDR)*. Accessed: Oct. 30, 2019. [Online]. Available: http://www.qwed.com.pl/resonators_spdr.html

[7] J. Krupka, "Frequency domain complex permittivity measurements at microwave frequencies," *Meas. Sci. Technol.*, vol. 17, no. 6, pp. R55–R70, Jun. 2006.

[8] J. Baker-Jarvis, *Transmission/Reflection and Short-Circuit Line Permittivity Measurements*. Boulder, CO, USA: National Institute of Standard and Technology, 1990.

[9] Agilent Technologies. (2005). *Basics of measuring the dielectric properties of materials*. Accessed: Oct. 6, 2019. [Online]. Available: academy.cba.mit.edu/classes/input_devices/meas.pdf

[10] C. K. Campbell, "Free–space permittivity measurements on dielectric materials at millimeter wavelengths," *IEEE Trans. Instrum. Meas.*, vol. 27, no. 1, pp. 54–58, Mar. 1978.

[11] W. Liu, L. Xu, X. Yang, Y. Shi, and H. Zhan, "Complex permittivity determination based on a radio frequency device," *Sens. Actuators A, Phys.*, vol. 272, pp. 75–82, Apr. 2018.

[12] V. Varadan, R. Hollinger, D. Ghodgaonkar, and V. Varadan, "Free-space, broadband measurements of high-temperature, complex dielectric properties at microwave frequencies," *IEEE Trans. Instrum. Meas.*, vol. 40, no. 5, pp. 842–846, Oct. 1991.

[13] A. A. Abduljabar, D. J. Rowe, A. Porch, and D. A. Barrow, "Novel microwave microfluidic sensor using a microstrip split–ring resonator," *IEEE Trans. Microw. Theory Techn.*, vol. 62, no. 3, pp. 679–688, Mar. 2014.

[14] M. H. Zarifi, A. Gholidoust, M. Abdolrazzaghi, P. Shariaty, Z. Hashisho, and M. Daneshmand, "Sensitivity enhancement in planar microwave active-resonator using metal organic framework for CO2 detection," *Sens. Actuators B, Chem.*, vol. 255, pp. 1561–1568, Feb. 2018.

[15] M. Abdolrazzaghi, M. Daneshmand, and A. K. Iyer, "Strongly enhanced sensitivity in planar microwave sensors based on metamaterial coupling," *IEEE Trans. Microw. Theory Techn.*, vol. 66, no. 4, pp. 1843–1855, Apr. 2018.

[16] A. A. Mohd Bahar, Z. Zakaria, S. R. Ab Rashid, A. A. M. Isa, and R. A. Alahnomi, "High–efficiency microwave planar resonator sensor based on bridge split ring topology," *IEEE Microw. Wireless Compon. Lett.*, vol. 27, no. 6, pp. 545–547, Jun. 2017.

[17] B. D. Wiltshire and M. H. Zarifi, "3-D printing microfluidic channels with embedded planar microwave resonators for RFID and liquid detection," *IEEE Microw. Wireless Compon. Lett.*, vol. 29, no. 1, pp. 65–67, Jan. 2019.

[18] M. H. Zarifi, "Sensitivity and selectivity enhancement in coupling ring resonator sensors using splitting resonant frequencies," in *IEEE MTT-S Int. Microw. Symp. Dig.*, Jun. 2018, pp. 36–39.

[19] W. Liu, X. Yang, Y. Niu, and H. Sun, "Improve planar multiple split-ring sensor for microwave detection applications," *Sens. Actuators A, Phys.*, vol. 297, Oct. 2019, Art. no. 111542.

[20] C.-K. Lee, "Evaluation of microwave characterization methods for additively manufactured materials," *Designs*, vol. 3, no. 4, p. 47, Sep. 2019.

[21] A. M. Nicolson and G. F. Ross, "Measurement of the intrinsic properties of materials by time–domain techniques," *IEEE Trans. Instrum. Meas.*, vol. 19, no. 4, pp. 377–382, Nov. 1970.

[22] W. B. Weir, "Automatic measurement of complex dielectric constant and permeability at microwave frequencies," *Proc. IEEE*, vol. 62, no. 1, pp. 33–36, Jan. 1974.

[23] F. Costa, C. Amabile, A. Monorchio, and E. Prati, "Waveguide dielectric permittivity measurement technique based on resonant FSS filters," *IEEE Microw. Wireless Compon. Lett.*, vol. 21, no. 5, pp. 273–275, May 2011.

[24] J. C. Vardaxoglou, *Frequency Selective Surfaces—Analysis & Design*. Taunton, UK: Research Studies Press, 1997.

[25] B. A. Munk, *Frequency Selective Surfaces: Theory and Design*. New York, NY, USA: Wiley, 2000.

[26] J. D. Ortiz, J. D. Baena, V. Losada, F. Medina, R. Marques, and J. A. Quijano, "Self–complementary metasurface for designing narrow band pass/stop filters," *IEEE Microw. Wireless Compon. Lett.*, vol. 23, no. 6, pp. 291–293, Jun. 2013.

[27] D. S. Lockyer, J. C. Vardaxoglou, and R. A. Simpkin, "Complementary frequency selective surfaces," *IEE Proc.-Microw. Antennas Propag.*, vol. 147, no. 6, pp. 501–507, 2000.

[28] D. Wang, W. Che, Y. Chang, K.-S. Chin, and Y. L. Chow, "A low-profile frequency selective surface with controllable triband characteristics," *IEEE Antennas Wireless Propag. Lett.*, vol. 12, pp. 468–471, 2013.

[29] X.-D. Hu, X.-L. Zhou, L.-S. Wu, L. Zhou, and W.-Y. Yin, "A miniaturized dual-band frequency selective surface (FSS) with closed loop and its complementary pattern," *IEEE Antennas Wireless Propag. Lett.*, vol. 8, pp. 1374–1377, 2009.

[30] H. Wang, M. Yan, S. Qu, L. Zheng, and J. Wang, "Design of a self-complementary frequency selective surface with multi-band polarization separation characteristic," *IEEE Access*, vol. 7, pp. 36788–36799, 2019.

[31] C. A. Balanis, *Antenna Theory Analysis and Design*, 3rd ed. Hoboken, NJ, USA: Wiley, 2005.

[32] S.-W. Lee, G. Zarrillo, and C.-L. Law, "Simple formulas for transmission through periodic metal grids or plates," *IEEE Trans. Antennas Propag.*, vol. AP-30, no. 5, pp. 904–909, Sep. 1982.

[33] S. S. Bukhari, W. G. Whittow, J. C. Vardaxoglou, and S. Maci, "Equivalent circuit model for coupled complementary metasurfaces," *IEEE Trans. Antennas Propag.*, vol. 66, no. 10, pp. 5308–5317, Oct. 2018.

[34] D. M. Pozar, *Microwave Engineering*, 4th ed. Hoboken, NJ, USA: Wiley, 2012.

[35] S. S. Bukhari, "Aritificial materials for microwave applications," Ph.D. dissertation, Wolfson School, Loughborough Univ., Loughborough, U.K., 2016.

[36] C. K. Lee, S. S. Bukhari, J. C. Vardaxoglou, and W. G. Whittow, "Optimisation of the Q factor of a complementary frequency selective surface," in *Proc. Loughborough Antennas Propag. Conf.*, 2017.

[37] Rogers Corporation. (2019). *RO4350BTM Laminates*. Accessed: Oct. 6, 2019. [Online]. Available: https://www.rogerscorp.com/acs/products/55/RO4350B-Laminates.aspx
[38] Taconic Advanced Dielectric Division. (2019). *TLX*. Accessed: Oct. 6, 2019. [Online]. Available: http://www.taconic.co.kr/download/TLX.pdf
[39] Rogers Corporation. (2019). *RO4360G2TM Laminates*. Accessed: Oct. 6, 2019. [Online]. Available: https://www.rogerscorp.com/acs/products/56/RO4360G2-Laminates.aspx
[40] Taconic Advanced Dielectric Division. (2019). *CER-10*. Accessed: Oct. 6, 2019. [Online]. Available: https://www.4taconic.com/page/cer-10-317.html

CHIH-KUO (CHUCK) LEE is currently pursuing the Ph.D. degree with the Wolfson School of Mechanical, Electrical and Manufacturing Engineering, Loughborough University, U.K. His research interests include periodic structures, metasurfaces, and dielectric properties measurements.

SHIYU ZHANG received the M.Sc. degree from the University of Manchester, U.K., in 2010, and the Ph.D. degree from Loughborough University, U.K., in 2014. After graduation, he was a Research Associate with Loughborough University, where he is currently with the Wolfson School of Mechanical, Electrical and Manufacturing Engineering. His research interests include additive manufacturing (3D-printing) antennas and RF circuit components, metamaterials, heterogenous artificial dielectrics, and wearable antennas and electronic systems. He received the EPSRC Doctoral Prize Research Fellowship Award, in 2015, carried out research on additive manufacturing 3D antennas and metamaterials.

SYED SHEHERYAR BUKHARI received the Ph.D. degree in electronics and electrical engineering from Loughborough University, U.K., in 2017. He is currently with the Department of Materials, University of Oxford, U.K. His research interests include periodic structures, metasurfaces, computational electromagnetics, artificial dielectrics, and additive manufacturing.

DARREN CADMAN received the Ph.D. degree from the Institute of Microwaves and Photonics, University of Leeds, U.K., in 2003, that investigated the optical control of microstrip electromagnetic bandgap structures. In 2007, he was with Filtronic Compound Semiconductors Ltd., where he took up the post of managing the Innovative Electronics Manufacturing Research Center based at Loughborough University, Loughborough, U.K. In 2016, he took up the post of Program Manager for the U.K.'s EPSRC funded project Synthesizing 3-D Metamaterials for RF, microwave, and terahertz applications led by Loughborough University. His current research interest includes the application of additive manufacturing processes to create microwave passive componentry.

J. (YIANNIS) C. VARDAXOGLOU (Fellow, IEEE) received the B.Sc. degree in mathematical physics and the Ph.D. degree in electronics from the University of Kent, U.K., in 1982 and 1985, respectively. He joined Loughborough University, U.K., as a Lecturer, in 1988, where he was promoted to a Senior Lecturer, in 1992, and a Professor of wireless communications, in 1998. He has served as the Dean of the School of Electronic, Electrical and Systems Engineering, Loughborough University, from 2011 to 2012. He established the Wireless Communications Research Group, Loughborough University, and founded the Centre for Mobile Communications Research. He is also the Director of Symeta Research Centre, funded by an EPSRC Grand Challenge Award, researching in a wide-ranging topic applicable to cutting-edge wireless communications technology. He collaborates with many internationally leading companies and universities. He is currently the Technical Director of Antrum Ltd., Loughborough, U.K. He has served as a Consultant to various industries and holds six patents. He has published over 300 refereed journals and conference proceeding papers (with 6500 citations) and has written a book on FSS. He was elected as a Fellow of the Royal Academy of Engineers, in 2011. His research interests include metamaterial structures and additive manufacturing (3-D printing) for RF/micro-/millimeter-wave engineering. He received a prestigious EPSRC's Grand Challenge č5M (FEC) Award: Synthesizing 3D Metamaterials for RF, Microwave and THz Applications. He has attracted research funding from industry and has been awarded 18 EPSRC research grants. He was Chairman of the Executive Committee of the IET's Antennas and Propagation Professional Network in the U.K. He chaired the IEEE's Distinguished Lecturer Program of the Antennas and Propagation Society for five years. He has chaired numerous IEE/IET events and has served on the Steering Committee of the European Conference on Antennas and Propagation (EuCAP). He also founded the Loughborough Antennas and Propagation Conference (LAPC), which has been running, since 2005.

WILLIAM G. WHITTOW (Senior Member, IEEE) received the B.Sc. degree in physics and the Ph.D. degree in computational electromagnetics from the University of Sheffield, Sheffield, U.K., in 2000 and 2004, respectively. From 2004 to 2012, he was a Research Associate with Loughborough University, Loughborough, U.K. In 2012, he became a Lecturer of electronic materials integration, University of Loughborough. He became a Senior Lecturer and a Reader of radio frequency materials with the Wolfson School of Mechanical, Electrical and Manufacturing Engineering, Loughborough University, in 2014 and 2018, respectively. He has authored more over 180 peer-reviewed journal and conference papers in topics related to electromagnetic materials, synthetic dielectrics, dielectric measurements, 3-D printing, wearable antennas, VHF antennas, specific absorption rate, finite-difference time domain, specific absorption rate, metamaterials, heterogeneous substrates, embroidered antennas, inkjet printing, electromagnetic compatibility, RFID tags, phantoms and genetic algorithms. He was the Coordinating Chair of the Loughborough Antennas and Propagation Conference (LAPC), from 2007 to 2011. In 2017, he received the Women's Engineering Society Award Men as Allies. He serves on the technical program committees of several IEEE international conferences. He has been asked to give 13 invited conference presentations; a four-day invited workshop on bioelectromagnetics and teach about dielectric measurements at the European School of Antennas. He is also an Associate Editor of the *Electronics Letters*.